ACUSTICA · acta acustica
Vol. 84 (1998) 801 – 814

Acoustic Detection of Gas Bubbles in a Pipe

T. G. Leighton, D. G. Ramble, A. D. Phelps, C. L. Morfey, P. P. Harris
Institute of Sound and Vibration Research, University of Southampton, Highfield, Southampton SO17 1BJ, UK

Summary
This report describes an acoustic system designed to detect gas bubbles in a pipe. The system makes simultaneous use of multiple techniques for detection and sizing; these include six resonance-based indicators, as well as off-resonance scattering. The abilities of these acoustic indicators to detect, size and count bubbles are compared. It was envisaged that using several simultaneous bubble detection techniques would compensate for restrictions inherent in the isolated use of individual techniques. For example, whilst geometric scattering tends to be more successful at locating bubbles than sizing them, the converse tends to hold for techniques which exploit the bubble resonance. In the latter case, the greater the tolerance allowed in the estimation of the bubble size from the measured resonance frequency, the more approximate may be the conversion algorithm. Single bubbles tethered to a wire in the pipe, and a freely rising stream of similar size bubbles, are examined. Results measured in these two cases are presented to indicate the potential of the location and sizing techniques. The effect on bubble resonance frequencies of confining the bubble in a pipe is considered in detail. Standard interpretations of bubble resonances in terms of bubble size assume free-field conditions, and require modification for the pipe environment. The necessary corrections are presented for the frequency range below the first transverse acoustic resonance of the pipe.
PACS no. 43.35.Yb, 43.30.Gv, 43.30.Es

1. Introduction

The ability to detect stable gas bubbles in a liquid is important to a range of applications [1, 2]. These include filling processes [3], material production (e.g. photographic industry), biomedical [4] and environmental applications [5, 6]. It may be necessary to ensure the absence of bubbles (e.g. in the glass industry), or their presence (e.g. in the production of certain food products). To further know the bubble size distribution present may in the first case assist in diagnosing the product fault which introduces the bubbles, and in the second case provide a quality check. In addition, where such stable bubbles are present, they may need to be characterised to assess the likelihood of inertial cavitation. This can be 'seeded' by stable bubbles in liquids subjected to high-amplitude pressure fluctuations (either acoustic or hydrodynamic) [7, 8, 9, 10]. Many such applications would involve the detection of bubbles in pipes, ranging from the very large (e.g. in the petrochemical industry) to the very small (e.g. blood vessels).

The choice of technique will depend on the information required, which is often case-specific. In many industrial situations, an over-sophisticated measurement system is unwanted because of implications for cost, ruggedness, and operator expertise: a simple discrimination between no-bubbles and some-bubbles may suffice. Systems have been designed which differ in the information they provide. This might be a measurement of the total gas/liquid interface present in the pipe, irrespective of how it is distributed amongst bubbles [11]. Alternatively ultrasonic imaging might detect bubble position or motion [12].

Perhaps the earliest techniques for bubble detection in a pipe used so-called 'geometrical' scattering of ultrasound off bubbles. Strictly, geometrical scattering occurs when the wavelength of the incident sound (λ) is much smaller than the lengthscale (ξ) associated with the scatterer (i.e. $k\xi \gg 1$ where $k = 2\pi/\lambda$ is the wavenumber of the sound). When ultrasound of order MHz is used to detect macroscopic air bubbles in water, then this limit may approach unity, and so the spatial resolution of the technique is often poor. One of the first experimental studies for using such scattering in bubble sizing was carried out by Nishi [13], who used a transmitter-receiver transducer pair operating at 5 MHz in continuous-wave mode to measure bubble sizes ranging from 100–600 μm. The excitation frequency was significantly greater than the resonance frequency of the bubbles and the incident sound was scattered from the bubble target. In addition, the transducer pair was angled to the direction of bubble flow which meant that a Doppler shift was imposed on the reflected signal. The method could therefore distinguish between reflections from stationary and moving objects. The simplicity of this technique has led to its application in measuring bubble size and velocity in two-phase flows in pipes [14, 15]. A major drawback with continuous-wave insonification is that at least two transducers are required. It is also not possible to obtain any depth information, and measurements can only be obtained in the beam overlap of the transmitting and receiving transducers. Also, if the geometry of the application means that sound energy cannot easily escape, there is a possibility that a reverberant field will build up which would mask the directly reflected signal. For this reason, alternative pulse-echo methods have been adopted. From knowledge of the transit time of the pulse and speed of sound propagation in the medium, the position of the bubble can be calculated. Belcher [16] used pulsed ultrasound to study decompression sickness. MacKay and Rubisson [17] used 7.5 MHz pulses to image bubbles resulting from decompression, in vivo in

Received 31 January 1997,
accepted 16 March 1998.

ACUSTICA · acta acustica
Vol. 84 (1998)

guinea pigs, fish and humans. Bubbles in guinea pigs were also detected by Watmough *et al.* [18], using a linear focused scanner which emitted pulses at 20 MHz. In industrial applications, Matikanien *et al.* [19]; Stravs *et al.* [20] and Chang and Morala [21] investigated the relative size distributions in pipes carrying two-phase mixtures. They deployed a single transducer emitting pulsed ultrasound which was either attached to the outside of the pipe or actually integrated into the pipe wall. Stravs *et al.* [20] using statistical methods in the analysis of large samples of pulse responses argued it might be possible to determine the relative bubble size distribution from the amplitude of the received echo.

Pulse-echo methods in pipes, of typical diameter of the order of 100 mm, usually use ultrasound of the order of a few MHz, which in water has a wavelength of a few mm. In such cases, it is evident from basic acoustic theory that the high frequency beam will not diffract significantly across the diameter of the pipe and so the ultrasound will remain in a narrow beam. This factor is important when it is required to detect bubbles across the whole pipe cross-section. However, with the advent of faster computer processing, techniques involving multiple transducers have been adopted. For example, Kolbe *et al.* [22] and Turko *et al.* [23] used an array of 20 transducers resonant at 10 MHz attached to the perimeter of a stainless steel pipe of inner diameter 57.5 mm. Although this system could provide a real-time image across the pipe it was only effective in measuring the size of large bubbles of diameter around 10 mm.

Norton and Linzer [24] and Norton [25, 26] presented a back-projection tomographical method. They showed that a two-dimensional acoustic reflectivity function could be defined within the interior of a circle. This could be done by acquiring reflectivity data from acoustic pulses transmitted by omnidirectional elements distributed around the circumference of the circle, and recording the resulting time-dependent backscattered sound. The pulse-echo data could be regarded as line integrals of the reflectivity function defined over circular arcs. These would be centred at points lying on the circumference of the enclosing circle. In an attempt to apply this theory to measure the void fraction of two-phase flows in pipes, Gai [27] constructed a 30 element array around the circumference of a pipe. Using polymethylmethacrylate lenses attached to the ultrasonic transducers, Gai managed to produce a diverging fan-shaped sound field. Wiegand and Hoyle [28, 29] applied parallel processing transputer architecture to apply the backprojection image reconstruction algorithm to the received data as each transducer in the array was sequentially pulsed. The end result was a real-time image of streams of bubbles, but no information was given on the accuracy of the individual size of the measured bubbles. The main drawback of this method is the complexity and expense of the associated hardware.

Additional pulse-echo methods applied to two-phase flows in pipes were carried out by Morris and Hill [12] who used a commercial medical ultrasound sector-scan probe coupled to the pipe using ultrasound gel. The sector-scan probe consists of a transducer element enclosed in an oil-filled dome. In this, it oscillates through an arc of 80 degrees, allowing an 80 degree sector of the pipe to be imaged in real-time. Blackledge [30] also used a commercial medical ultrasound probe (a linear array of 132 transducer elements producing a sequence of 7.5 MHz pulses). The probe was coupled via gel along the length of pipe. The ultrasound image of the flow was then captured by a frame-grabber and image-processing techniques were applied to assess the void fraction of the flow. Both these techniques could provide real-time image of the flow, accurate velocity data but not accurate bubble size data. Pulse-echo methods have also been used to detect bubbles in the ocean: Thorpe and Hall [31] used a dual-beam side-scan sonar to obtain information on the formation and evolution of bubble clouds in the ocean.

The above techniques illustrate that, when there exists a significant impedance mismatch between the liquid and the gas, and the wavelength of sound is small compared to the size of the bubble, then a degree of bubble detection can be achieved from the scattered component of an incident sound field. Backscattering causes an acoustical shadow to be cast behind the bubble. This, and other sources of loss, cause beam attenuation. Chang *et al.* [32] and Stravs and Stockar [33] used two ultrasound transducers, placed on opposite sides of a pipe, to measure the attenuation caused by the presence of bubbles in the flow. However, only crude estimates of the actual bubble size could be obtained by recording the relative amounts of attenuation by different sizes of bubbles. Wolf [11] extended this principle with a circular array of 108 transducers directly integrated into the wall of a 140 mm diameter pipe. Each transducer in turn produced a 5 MHz pulse and the opposite transducer recorded the amount of ultrasound received. The data was processed to give a real-time measure of the total surface area of bubble interface in the population as a function of position within the cross-section of the pipe. The technique could only resolve bubbles of radius approximately 2.5 mm or greater.

In summary, non-resonant scattering and attenuation techniques for bubble detection have had many applications. They are able to detect and locate an inhomogeneity in the liquid providing the gas-liquid impedance mismatch is large enough and that the wavelength of the sound sufficiently small compared to the size of the inhomogeneity. However, the principal drawbacks are: they are insensitive to the nature of the inhomogeneity, so that in practice they may not distinguish between bubbles and solid bodies of a similar size; they cannot detect the difference between the scattering from a large bubble and that from a cluster of smaller ones; and they cannot accurately measure the size of the bubbles present. Therefore, to overcome these problems additional techniques may be used which make use of the strong acoustical resonance characteristics exhibited by bubbles.

The pulsation of a bubble approximates to a lightly damped single degree of freedom system, where the inertial component arises mainly from the much denser liquid surrounding the bubble; the stiffness is attributable to the compressibility of the gas inside the bubble; and the damping is brought about through viscous losses at the bubble wall, sound radiated into the fluid and thermal losses. As such it has a well defined resonance frequency, which for an air bubble in a

large body of water at atmospheric pressure can be approximately expressed as [34]:

$$\nu_0 R_0 \approx 3.2 \quad \text{Hz m}, \tag{1}$$

where ν_0 is the resonance frequency and R_0 is the equilibrium bubble radius (valid for $R_0 \gtrsim 10\,\mu$m). Therefore from a knowledge of the acoustic resonance frequency of a bubble, an estimate of its size can be made. However the greater the accuracy required of the estimation of bubble size, the more rigorous must be the corrections for the case specific to the bubble. There are well-documented corrections for surface tension, viscosity, gas properties, static pressure etc. relating to an isolated bubble in an infinite medium [7, 1], as well as those relating to the presence of other bubbles, interfaces, or walls [35, 36, 37, 38]. In this paper, we recognise that further corrections to equation (1) are required because the bubble is in a pipe, as opposed to free space; these are discussed in section 4.3. Until then, any indication of bubble size will be given in terms of the resonance frequency only, which is completely adequate for the no-bubbles/some-bubbles distinction discussed above.

It is possible to measure the resonance frequency directly by observing the strength of a backscattered acoustic signal, using a driving signal here termed the *pump* signal, of angular frequency ω_p. However such estimates have poor spatial resolution for bubble location, as at resonance the radii of bubbles are orders of magnitude smaller than the wavelength of the sound field; and provide ambiguous results, in that a bubble much larger than resonance may scatter more sound than a small resonant bubble [39, 1]. This ambiguity may by reduced by monitoring the nonlinear behaviour of a bubble, which tends to increase at resonance as the amplitude of oscillation increases. This results in the generation of integer related harmonics of the driving signal frequency at $2\omega_p, 3\omega_p$ etc., and non-integer harmonics of the sound field, typically a subharmonic at $\omega_p/2$ and ultraharmonics at $3\omega_p/2, 5\omega_p/2$ etc. [40].

The long-term objective of this research was to provide an acoustical system which could analyse gas bubbles in liquids in a pipe, in order first to determine the range of bubble resonances present in the region of pipe sampled; and second to provide information on the spatial location of the bubbles within the pipe cross-section. With respect to bubble location, increased spatial resolution can be achieved through the use of higher frequencies. As stated above, 'geometric' techniques tend to be much better at locating bubbles than sizing them, whilst the converse is true of resonance techniques which use a pump signal alone. Clearly, by using the two simultaneously, both measurements can be obtained (a process which is done in this paper). However the two general approaches can be combined in another way, the so-called 'two-frequency' technique, which has one important advantage not afforded by the first approach. Specifically, it allows a small region of the pipe to be sampled for bubbles, which offers in principle the option of obtaining an estimate of the number of bubbles from the strength of the signal scattered by them. This is because such counting depends on knowledge of the amplitude of the pump signal [41]. Whilst in general this will not be constant throughout the volume of the pipe, the two-frequency technique allows a sample volume (within which bubbles are to be measured) to be selected within the pipe. Its volume can be controlled, and made small enough to ensure that within it the amplitude of the pump sound field is constant to within the desired tolerance. This issue will be re-examined in section 4.2.

The two-frequency technique operates as follows. The bubble is insonified by a high frequency fixed *imaging* beam (at angular frequency ω_i) and the lower frequency *pump* beam at angular frequency ω_p tuned to the resonance frequencies of the bubbles under investigation. A range of combination frequency signals is subsequently generated by the bubble, the amplitude of each component tending to a maximum at resonance. This ranges includes signals at $\omega_i \pm \omega_p$ and at $\omega_i \pm \omega_p/2$. In sparse, slow-moving populations the $\omega_i \pm \omega_p/2$ signal gives the better radius resolution and the least ambiguity [42]. However providing the bubbles are moving rapidly enough to generate a sufficiently large Doppler shift to allow the contributions from bubble scattering to be differentiated from other sources of nonlinearity (e.g. turbulence), the $\omega_i \pm \omega_p$ is more useful for counting bubbles at higher population densities [41]. The use of combination frequencies therefore allows identification of the bubble resonances. The combination frequencies themselves are at frequencies close to $\omega_i/2\pi$ (which equals 2.25 MHz in this experiment), so that this technique moves the detection signal from around the resonance to a frequency window of, usually, lower ambient noise.

However, although the use of the high frequencies in this technique conveys these advantages, it measures only the bubbles passing through the focus of the high frequency projector and receiver transducers. It is not therefore capable of readily allowing localisation of bubbles anywhere across the pipe section. To do this, a further technique had to be used in conjunction. This problem of spatial resolution was addressed through the use of a 3.5 MHz ultrasonic scanner, whose operational frequency is much higher than any potential bubble resonance. This will show a signal at the location of any impedance mismatch across the pipe section, typically from a bubble or possibly a solid inhomogeneity.

Such a use of several simultaneous techniques for bubble detection has been termed COBUST ("Characterisation of Bubbles Using Simultaneous Techniques"). Potentially it can allow compensation for the limitations of any one technique through the use of the others. In addition to the 3.5 MHz ultrasonic scanner, a range of signals which relate to the bubble resonance were generated, as follows. When insonified by both pump (ω_p) and imaging (ω_i) frequencies, the oscillating bubble may emit a wide spectrum of signals ($\omega_p, 2\omega_p, \omega_p/2$, $\omega_i \pm \omega_p, \omega_i \pm 2\omega_p, \omega_i \pm \omega_p/2$ etc.). The simultaneous analysis of all these signals can be optimised to estimate the radii of the bubbles in the population. Following the significant success of the technique in tests performed in an approximately free field environment in a tank [43], COBUST was here deployed in a pipe to locate bubbles within the pipe cross-section, and indicate their resonance frequencies.

ACUSTICA · acta acustica
Vol. 84 (1998)

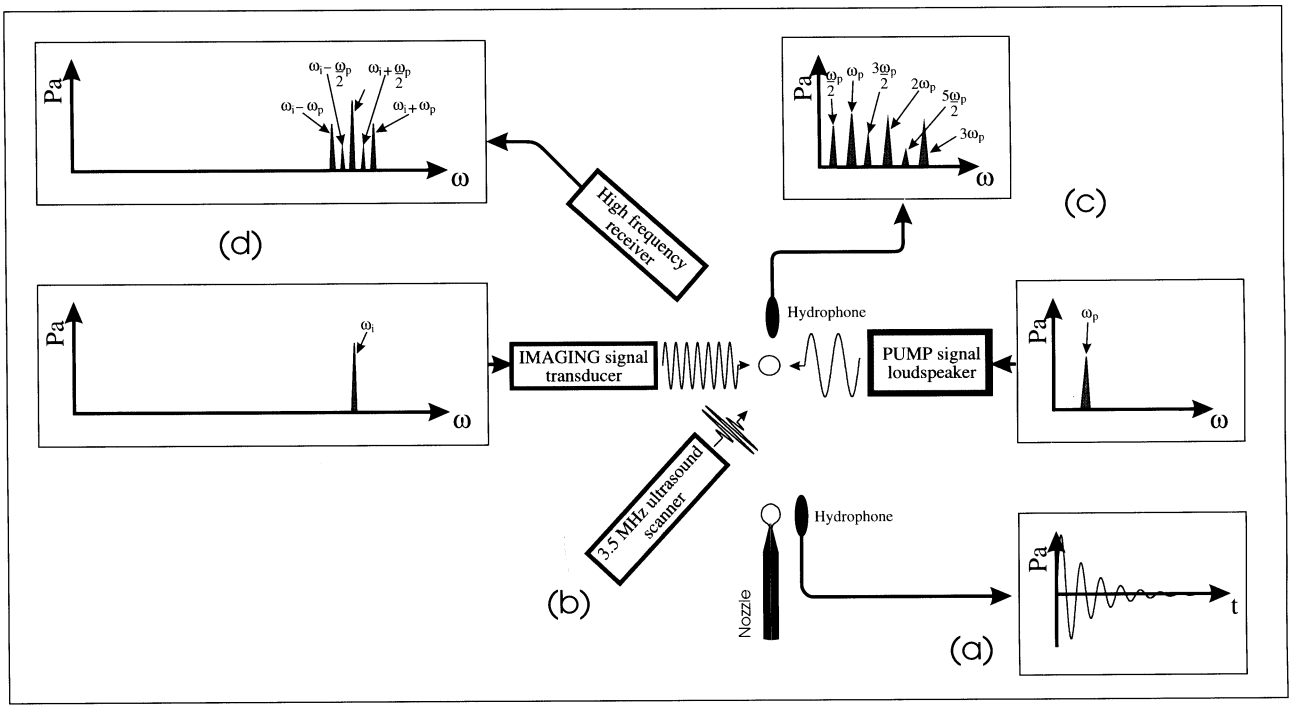

Figure 1. Schematic of the apparatus required to implement the various acoustic detection techniques. In (a) the bubble is shown, injected from a nozzle, where a hydrophone detects its short duration passive emissions. In contrast, all the active techniques are schematically shown interrogating a bubble which has risen under buoyancy. In (b) a medical diagnostic ultrasound scanner is deployed to produce an image of the bubble (shown in Figure 2). In (c) the pump transducer generates a series of tonal pump signals, and a second hydrophone detects structure in the spectrum corresponding to $2\omega_p$, $3\omega_p$, $\omega_p/2$, $3\omega_p/2$ and $5\omega_p/2$ in the presence of a resonant bubble. In (d) a high frequency imaging signal is projected onto the bubble, and the scattered signal is detected by a high frequency receiver. Whilst in the absence of the bubble, ideally only ω_p and ω_i should be present, a resonant bubble will produce structure in the spectrum around ω_i [40].

2. Method

The principle by which COBUST operates is that the accuracy, sources of ambiguity and other limitations inherent in each individual bubble presence / size indicator are investigated and compared through simultaneous deployment. In this way, it is hoped that additional information may be obtained through the examination of two or more signals which would compensate for the limitations in any one technique. For example, if a liquid containing bubbles is insonified with a pump frequency ω_p, then strong scattering at ω_p may be the result of resonant bubbles, or may be the result of geometrical scattering from large bubbles [2]: used on its own, there is no way to distinguish between these two returned signals. The contrast between the information available in geometrical and resonant techniques has already been made.

The generic COBUST apparatus is shown schematically in Figure 1 [40]. Upon injection from a nozzle the bubble may be sized from its passive acoustic emissions (an exponentially-decaying sinusoid shown in Figure 1a). The pump signal is generated at ω_p (by the Pump signal transducer) and the scattered spectrum analysed in terms of the harmonics, subharmonic and ultraharmonics (as shown in Figure 1c). By additionally introducing the high frequency *imaging* transmitter and receiver, the spectrum of combination frequencies can also be analysed, and the bubble presence inferred through the scattering of signals at $\omega_i \pm \omega_p$, $\omega_i \pm 2\omega_p$, $\omega_i \pm \omega_p/2$, etc. (Figure 1d). In addition geometrical scattering using a 3.5 MHz scanning system is shown in Figure 1b. Though the wavelength is in general not sufficiently small to obtain good radius resolution directly from the scanner, in previous tank tests, where the plane of the imaging beam is angled to the vertical, it has been possible to estimate the bubble radius from the rise time using this instrument [43]. However in the pipe it was not possible to angle the beam in this way, so that any motion information is useful only for the detection of transients (and therefore as a possible trigger for an automated detector), and for measuring the rate of injection of bubbles, and is not an accurate way of determining bubble size.

The specific experimental arrangement used for the pipe tests is shown schematically in Figure 2. The bubbles are injected at the base of the pipe, which has internal diameter of 104 mm, and their passive emissions are detected by the lower hydrophone (HP2). This is a Bruel and Kjaer type 8103 device, conditioned using a type 2635 preamplifier, and is used for sizing. They rise through the beam of the 3.5 MHz ultrasonic scanner (Hitachi EUB-26E), and are then driven by the pump signal, which is generated by the ring transducer. This consists of a 104 mm inner diameter by 6 mm thick PZT-4 (Lead Zirconate Titanate) piezo-ceramic ring which was set into a polyurethane foam and encased in a Nylon housing. The signal to the pump transducer was generated using a Tektronix AWG 2005 waveform generator (which was controlled via its GPIB interface by the PC), and this was passed though a Bruel and Kjaer type 2713A power

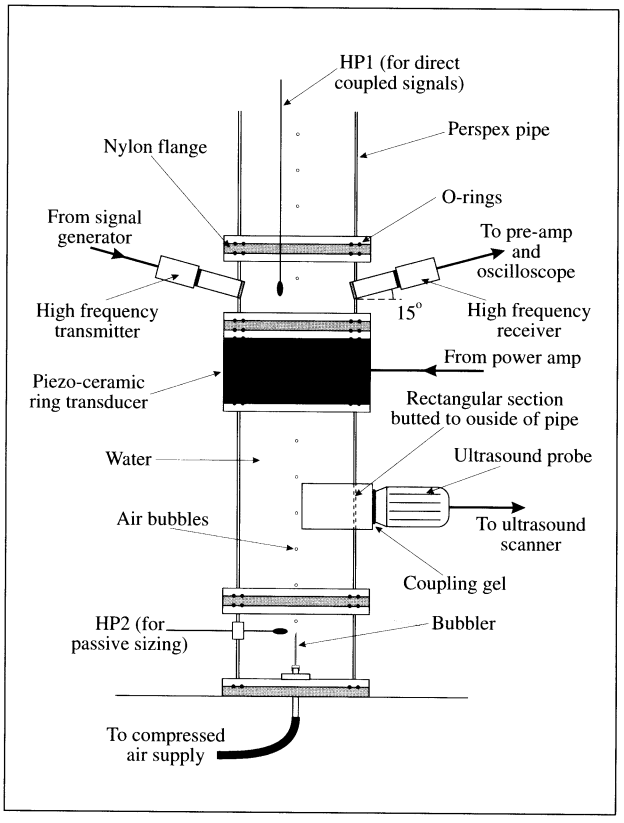

Figure 2. Schematic of the apparatus used in the measurements of bubbles in a pipe.

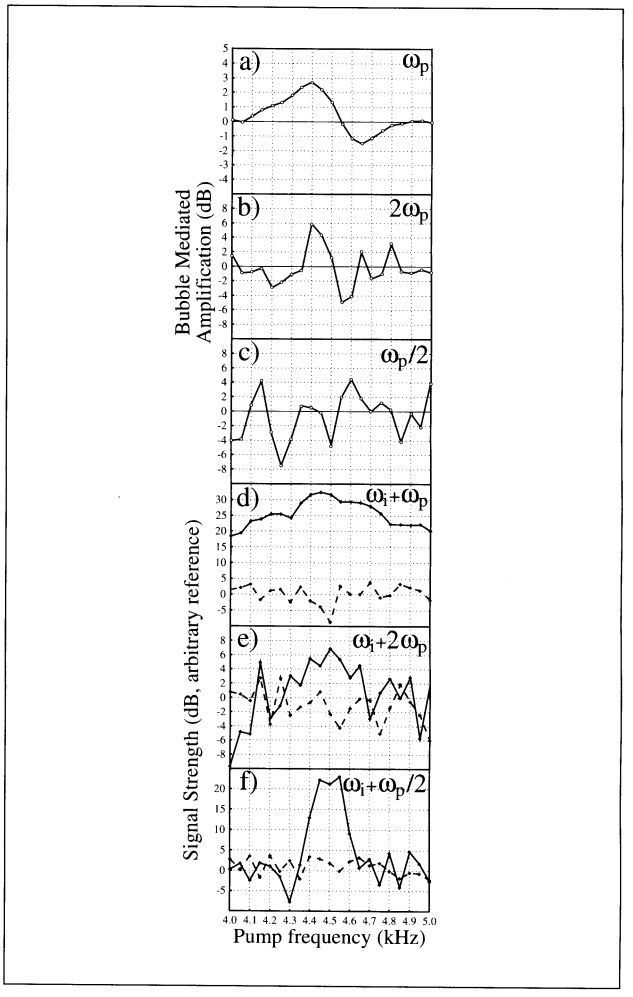

Figure 3. Results from measurements of a stationary bubble tethered to a wire in the transducer focus in the pipe. The bubble was insonified between 4 kHz and 5 kHz using consecutive tone-bursts of duration 0.2 s, incrementing the frequency in 50 Hz steps between bursts. This frequency range includes the tethered bubble's resonance frequency, and each tone was of amplitude 120 Pa. The signals shown are at: a) ω_p, b) $2\omega_p$, c) $\omega_p/2$, d) $\omega_i + \omega_p$, e) $\omega_i + 2\omega_p$ and f) $\omega_i + \omega_p/2$. For the scattering at ω_p, $2\omega_p$ and $\omega_p/2$ (i.e. parts a–c), the bubble-mediated amplification (i.e. the ratio of the 'bubble present' to 'bubble absent' signal levels) is plotted (solid line with open circles). For the $\omega_i + \omega_p$, $\omega_i + 2\omega_p$ and $\omega_i + \omega_p/2$ signals (i.e. parts d-f), the signal strength relative to the average noise floor is plotted when the bubble is present (solid line with crosses) and absent (broken line with crosses). Symbols (circles and crosses) are at data points.

amplifier to the transducer. The upper hydrophone (HP1), again a Bruel and Kjaer type 8103, can be incorporated into the pipe wall or, as shown in Figure 2, immersed in the liquid. It detects the scattering of the harmonics and subharmonics of the fundamental resonance.

The additional combination frequency measurements are achieved through the use of the two high frequency transducers, shown angled at 15° to the horizontal. In the actual set-up the transducers were inserted into the pipework 90° apart, although they are shown on opposite sides of the pipe in Figure 2 for clarity. The high frequency beam was generated using a Wavetec model 171 analogue signal generator, which was then amplified using an ENI model 240L RF power amplifier and output through a 2.25 MHz transducer, as manufactured by KB Aerotech. The scattered signal from the bubble was received using a second KB Aerotech transducer, and was then conditioned by a Panametrics type 5670 ultrasonic preamplifier. The beam patterns of the imaging frequency projector and receiver overlap within the region of the pipe surrounded by the ring transducer. In this way a focus (which bounds the region wherein the sound field amplitude does not fall more than 3 dB below its peak value), has volume 0.07 ml and is centred on the pipe axis. A preliminary calibration procedure (detailed in [43]) was performed to ensure that the amplitude of the pump signal in this sensing volume was constant for all pump frequencies.

The data acquisition was performed using a LeCroy type 9314L digital storage oscilloscope, which was again controlled and passed data to the PC via its GPIB interface. The signal from the two low frequency hydrophones HP1 and HP2 were connected straight into the oscilloscope. However, the high frequency signal from the KB Aerotech transducer and Panametrics preamplifier was additionally demodulated before sampling. This involved an analogue multiplication of the returned signal with a reference signal from the Wavetec signal generator - this has the effect of shifting all the useful sum-and-difference information contained around the imaging signal to just above dc, allowing much reduced sampling rates and data lengths.

ACUSTICA · acta acustica
Vol. 84 (1998)

3. Experimental results

As an initial test, a single bubble is tethered in the focal overlap region of the two high frequency transducers (details of tethering can be found in [43]). Its radius (after later detachment) was optically measured to be 0.7±0.1 mm. The signals simultaneously detected from it when ω_i is fixed, and ω_p is increased incrementally, are shown in Figure 3. The direct scattered signal at ω_p is presented in Figure 3a; $2\omega_p$ in Figure 3b; and $\omega_p/2$ in Figure 3c. The demodulated signals at $\omega_i+\omega_p$, $\omega_i+2\omega_p$ and $\omega_i+\omega_p/2$ are shown in Figures 3d to 3f respectively. All the signals are taken simultaneously as the pump signal output was varied from 4 to 5 kHz in consecutive tone-bursts of duration 0.2 s, incrementing the frequency by 50 Hz between bursts, and at an amplitude of 120 Pa. The bubble-mediated amplification (i.e. the ratio of the 'bubble present' to 'bubble absent' signal levels) is plotted for the scattering at ω_p, $2\omega_p$ and $\omega_p/2$, but because the MHz noise floor is so low (shown as broken lines in Figures 3d to 3f), the signal strength relative to the average noise floor is plotted for the $\omega_i + \omega_p$, $\omega_i + 2\omega_p$ and $\omega_i + \omega_p/2$ signals. The bubble resonance is best indicated by the $\omega_i + \omega_p/2$ signal to be 4500±50 Hz (in agreement, through equation (1), with the optical measurement). The $\omega_i + \omega_p$ signal peaks in this region but its frequency spread is much larger. In contrast, the $\omega_i + 2\omega_p$ signal, although it also peaks around 4500 Hz, does not rise sufficiently out of the noise to provide an unambiguous bubble indicator. The scatter of the fundamental, ω_p, shows the expected through-resonance behaviour, centred around 4500±100 Hz, but neither the second harmonic nor subharmonic signals reliably indicate the presence of a single bubble.

This trend in results continued when measurements were taken on rising bubbles, where any one signal alone provided a less clear picture of both the bubble size and location than the use of multiple signals. The bubbler itself consisted of a micro-syringe (Hamilton No. 701) connected to a compressed air supply. The air feed was additionally constricted near the location of the syringe, which allowed a continuous stream of similarly-sized bubbles to be generated [44]. Data taken when sizing a stream of rising bubbles is presented in Figures 4 to 6, with the direct scattered signals at ω_p, $2\omega_p$ and $\omega_p/2$ shown in Figures 4a to 4c respectively, and the demodulated combination frequency results (taken simultaneously) shown in Figure 5. Here, the bubble stream was insonified with the pump transducer between 3.5 and 4.5 kHz in 50 Hz steps, and at an amplitude of 150 Pa. From the direct scattered signals, only the result at ω_p (shown in Figure 4a) gives any indication of the bubbles' resonance, at 4000±200 Hz. In contrast the grey-scale plot of the power spectrum of the demodulated combination-frequency scattered signal (Figure 5) shows a clear peak in the $\omega_i \pm \omega_p/2$ signal at 3950±50 Hz, with a similar but less pronounced peak evident in the $\omega_i \pm \omega_p$ signal. At each signal location, the $\omega_i + \omega_p/2$ and $\omega_i - \omega_p/2$ signals are separately resolvable, as a result of the Doppler shift before demodulation. A similar effect is seen in the $\omega_i \pm \omega_p$ signals.

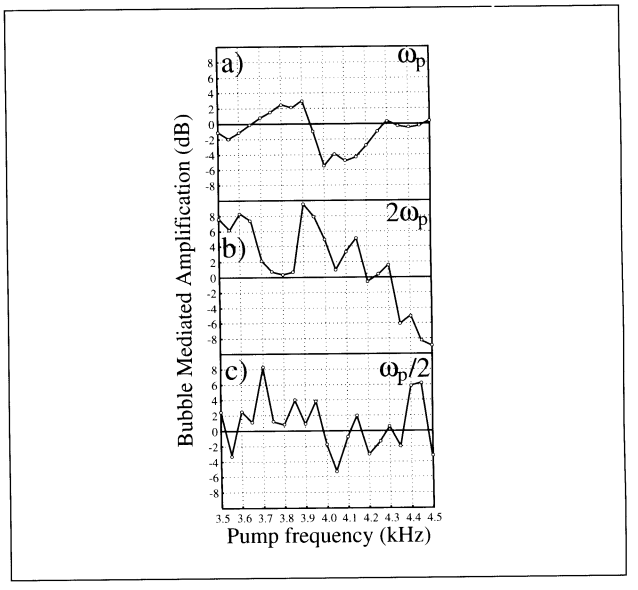

Figure 4. Low frequency backscattered results from measurements at a) ω_p, b) $2\omega_p$, and c) $\omega_p/2$, on rising bubbles (appropriate allowance having been made for Doppler effects). The bubbles were insonified between 3.5 and 4.5 kHz in 50 Hz steps at an amplitude of 150 Pa. The bubble-mediated amplification (i.e. the ratio of the 'bubble present' to 'bubble absent' signal levels) is plotted. Symbols (open circles) are at data points.

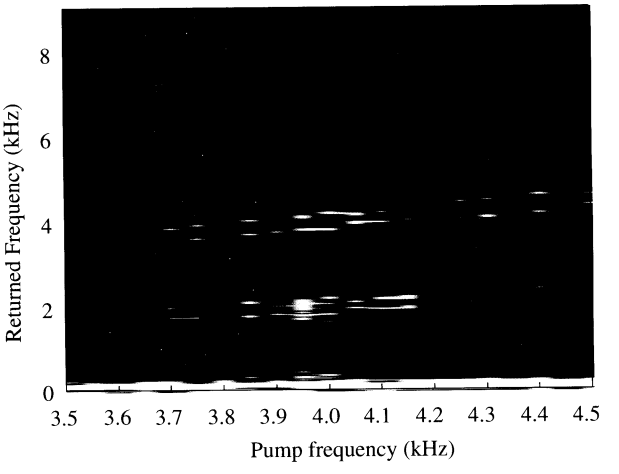

Figure 5. High frequency backscattered results taken simultaneously to the results shown in Figure 4. The grey-scale plot shows areas of high signal strength in white. The frequency spectra of the 'Returned' signal (which has been heterodyned), obtained for each setting of the pump frequency (shown on the horizontal axis), have been plotted side-by-side to form a single grey-scale representation, emphasising the changes in the spectral components. The sum-and-difference peaks are separated due to a Doppler shift on the returned signal.

Motion information is most clearly determined through the simultaneous M-mode operation of the 3.5 MHz ultrasound scanner, shown in Figure 6a, where the horizontal axis represents the time scale (of duration 2 s) for objects moving through the line shown in the centre of the B-mode image (Figure 6b). The ultrasound scanner displays B-mode and M-mode images simultaneously [45, 46]. The B-mode, or 'brightness'-mode (Figure 6b), displays in two spatial dimen-

sions the position of acoustic reflectors within the ultrasonic beam, the brighter pixels in general corresponding to the position of the strongest reflectors. With this arrangement of the transducer (Figure 2) it shows a horizontal cross-section of the pipe, the top of Figure 6b corresponding to the transducer faceplate. The distance from the faceplate is marked in centimetre divisions down the line dividing Figure 6b from 6a. The M-mode, or 'motion'-mode (Figure 6a) displays this single spatial dimension as a function of time (on the horizontal axis), indicating the passage of acoustic reflectors through the white line marker which bisects Figure 6b. Bubbles therefore show as almost vertical streaks in M-mode. In Figure 6b a bubble can be seen crossing the white line in the centre of the frame. This frame represents a horizontal cross-section of the pipe, the 18 cm distance in the field from the transducer face (which is at the top of the frame) being indicated by centimetre-spaced markings on the border between frames 'a' and 'b'. The curved wall of the pipe remote from the transducer can be seen in the lower half of frame 'b' where it is labelled 'P'. Below it is an intense horizontal white region indicating strong scattering from the pipe-air interface remote from the transducer (labelled 'A'). Using this geometric scattering technique, the location of the bubble can be determined as being at 74±3 mm in front of the face plate of the ultrasonic transducer head, along the diameter which runs perpendicularly between the centre of the faceplate and the extreme pipe wall.

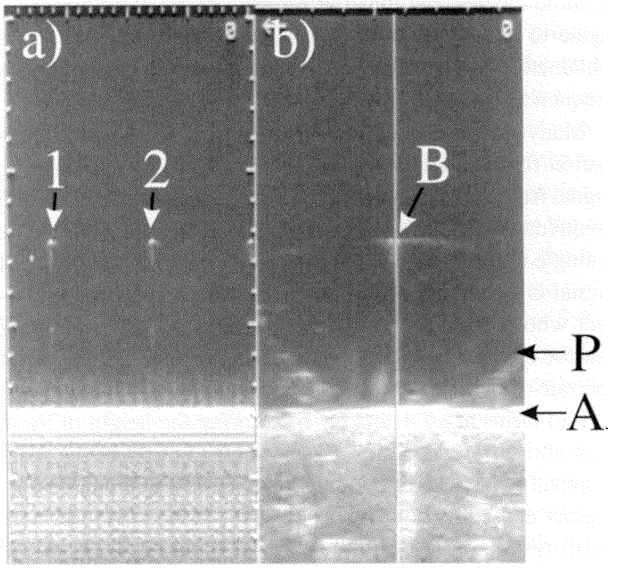

Figure 6. Results from the 3.5 MHz ultrasonic scanner. a) M-mode scan, recording (against time over a 2s period plotted on the horizontal axis) the position of images which cross the vertical white line in the centre of b) the B-mode image. Bubbles (1&2) therefore show as almost vertical streaks. In b) the bubbles (B) can be seen crossing the white line in the centre of the frame. This frame represents a horizontal cross-section of the pipe, the 18 cm distance in the field from the transducer face (which is at the top of the frame) being indicated by centimetre-spaced markings on the border between frames 'a' and 'b'. The curved wall of the pipe (P) remote from the transducer can be seen in the lower half of frame 'b', and below it is an intense horizontal white region (A) indicating strong scattering from the pipe-air interface remote from the transducer.

4. Discussion

4.1. Bubble detection using this system

The initial intention of the employment of the COBUST principle was to allow the ambiguities inherent in one technique to be partially compensated by using a second technique simultaneously. However, it is clear that certain resonance indicators do not yield a satisfactory measure of the bubble's resonance to warrant their inclusion in a generalised bubble sizer. A brief discussion of the various different techniques is now presented to identify the sinals most useful to sizing and counting an unknown bubble population.

It is clear from both the tethered and moving bubble tests that the direct backscattered signal at ω_p shows the resonant pulsation characteristics clearly, if not particularly accurately. This is to be expected as the sound field must simply drive the bubble into linear pulsation, and thus the behaviour of the bubble is highly predictable and can be easily estimated analytically. This signal (with $\omega_i + \omega_p$) may be particularly useful as it can be rapidly investigated across a range of frequencies using broadband insonification [40], a factor which becomes increasingly important for monitoring bubble populations which change on shorter timescales than the very stable ones used in this test. However, as mentioned earlier, the ω_p signal is not a global maximum at the resonance frequency of a bubble, and a larger bubble may scatter more sound as a result of geometric backscatter. Additionally, there is very poor spatial localisation using this (and any other non-combination frequency) technique, as the wavelength of the driving sound field is orders of magnitude higher than the radius of a bubble resonant at that frequency. This will prove to be a problem when bubble counting is required owing to the spatial variation of the pump signal within the pipe. In order to relate the height of the backscattered signal to the number of resonant or near-resonant bubbles at that frequency, it is necessary to know the pump acoustic pressure amplitude accurately, which may vary considerably because of the acoustic effects of the pipe wall. This will be discussed in more depth in section 4.2.

It is clear from Figures 3b, 3c, 4b and 4c that neither of the other two low frequency backscatter techniques, at $2\omega_p$ and $\omega_p/2$, demonstrates the same clarity of resonant behaviour as shown by the ω_p signal. The signals are a measure of two different nonlinearities in the acoustic bubble response. The signal at $2\omega_p$ is a measure of an asymmetry in the bubble volumetric pulsations. However, although the height of the $2\omega_p$ backscatter is a global maximum at the bubble resonance, it is very difficult to differentiate the signal from harmonic distortion in the signal generation and measuring equipment, and it is apparent that the strength of the bubble mediated $2\omega_p$ signal is not sufficiently large to allow it to be unambiguously identified in the returned signal. The other nonlinear signal, the subharmonic at $\omega_p/2$, is generated by surface waves on the bubble wall [42, 47]. These surface waves are a very lightly damped effect, and thus should allow a very accurate measure of the bubble resonance. However they involve no

ACUSTICA · acta acustica
Vol. 84 (1998)

volume change and thus the acoustic signal does not propagate to distance. For this reason, no useful information is obtained by examining the backscattered response at this frequency.

Many of these problems are resolved when the combination frequency techniques are employed. As the imaging signal frequency is orders of magnitude higher than the pump frequency, the bubble pulsation is effectively 'frozen' during a single imaging cycle, and thus the strength of the returned signal is a measure of the geometric scattering from an object whose cross-section varies periodically. This coupling has the effect of amplitude modulating the imaging signal at the rate of the pump / resonance frequency, with the generation of terms at $\omega_i \pm \omega_p$. By monitoring the height of these sum-and-difference terms, it is possible to measure the basic resonant behaviour of the bubble pulsations without the ambiguity caused by confusing large off-resonant bubbles with small resonant ones, as the height of the $\omega_i \pm \omega_p$ signal is a maximum at the bubble resonance. It also allows spatial localisation of the bubbles to within a sample volume in the liquid: if two high frequency transducers are used, one as a projector of the imaging frequency and the other to receive the scattered signal, only bubbles within the small intersection of the high frequency beams will be measured.

The same principle gives rise to the signals at $\omega_i \pm 2\omega_p$ and $\omega_i \pm \omega_p/2$, where the basic bubble behaviour causes an amplitude modulation of the high frequency imaging signal backscattered from the bubble. The acoustic signal at $\omega_i \pm \omega_p/2$ will now propagate to distance as the surface waves act solely to modulate the cross section of the bubble presented to the imaging signal beam. However, examination of the data shown in Figure 3e and Figure 5 show the $\omega_i \pm 2\omega_p$ signal again not to be reliable enough to warrant its inclusion in a generalised pipe bubble sizer.

Thus there are realistically two bubble resonance indicators which may be of benefit to the measurement of bubbles in the pipe - those at $\omega_i \pm \omega_p$ and $\omega_i \pm \omega_p/2$. Both of these signals examine the bubbles within a small sample volume, which (if the focus is sufficiently small) ensures that the effect of pump signal amplitude variation within the pipe is unimportant: the amplitude of the driving sound field at the high frequency focus can be easily determined over the range of pump frequencies required. However, the signal at $\omega_i \pm \omega_p/2$ must be interpreted with some caution. Although the signal is the most accurate and only unambiguous indicator of a resonant bubble which propagates to distance, it has many features which make it impractical as a bubble sizer. The phenomenon by which surface waves appear on the bubble wall is a parametric effect, that is the bubble must be driven with sound whose amplitude exceeds a well defined threshold [42]. Additionally, the height of the backscattered $\omega_i \pm \omega_p/2$ signal is unpredictable, such that in a bubble sizer / counter the appearance of such a signal must be related to a single bubble at resonance. The low damping associated with the surface wave effect means that the bubble must be driven for a number of cycles to allow any transients to decay away, which for a 3 kHz bubble is typically between 200 and 400 cycles [48]. In earlier experiments conducted on an oceanic bubble population which implemented this combination frequency technique [41], not one subharmonic signal was evident in the returned signals.

The deployment of COBUST in a pipe can be compared against an *Ideal objective* [49] which can be formulated for a bubble sizing system. The system would deploy a range of these techniques to interrogate a given liquid sample, either sequentially or concurrently as defined by the problem. This would enable optimisation of the process of characterising the bubble population in the liquid with respect to minimising the ambiguity of the result and the complexity of the task. The task itself involves first the detection of inhomogeneities in liquids. In certain circumstances it is then necessary to analyse the sample further to distinguish gas bubbles from solid or immiscible liquid-phase inclusions. The final stage of analysis would involve not only the detection, but also the sizing of the gas inclusions, leading to the characterisation of the bubble population. The *Ideal Objective* can therefore be summarised through the following goals:

i. Detect inhomogeneities in liquids.

ii. Distinguish gas bubbles from solids.

iii. Measure size of gas inclusions present.

iv. Measure number of bubbles in each size class.

As stated in the Introduction, case-specific considerations dictate how many of the four stages are required, desirable, or practicable. The pipe system discussed in this paper contains in principle the necessary basis for satisfying this objective. The first two criteria are satisfied as followed. As bubbles pass through the field of the Hitachi scanner, M-Mode operation indicates the presence of a moving body having a specific acoustic impedance significantly different from that of the liquid. Its position is recorded on the B-mode image, which will also roughly indicate the number of inhomogeneities, or whether there is a massive obstruction (such as an air plug). However geometrical scattering on its own cannot distinguish between solid and gaseous inhomogeneities, nor give an accurate measure of size. However the inhomogeneity then passes through the ring transducer, which can make the distinction: resonant scattering of the pump signal by a bubble is many orders of magnitude stronger than that from a solid body of similar size [39, 50]. In this test, therefore, the current system satisfies the first two components of the *Ideal Objective*. That is not to say this paper has demonstrated satisfaction of all four component requirements. It was a test experiment, which employed very simple bubble populations. Counting was indicated only through the M-mode image, the issue of the measurement of bubble size spectra (criterion iv) being demonstrated in principle through meeting the twin requirements of obtaining signals at $\omega_i \pm \omega_p/2$, and ensuring uniformity of the pump signal amplitude in the sample volume (see section 4.2). Additionally, both to satisfy criterion (iii) and to obtain the size spectra of (iv), it is necessary to relate the bubble resonance frequency to the bubble radius, an issue which is discussed in section 4.3.

4.2. The pressure field within the pipe

Certain issues are important when discussing the acoustic detection of bubbles in a pipe, as opposed to a free-field situation. Pressure waves, travelling in the z direction in an infinitely long pipe of circular cross-section, can be expressed as a series of modes [51]. The complex pressure contribution from a mode can be written as

$$p_{mn}(r,\vartheta,z) = A^{m,n} J_m(\kappa_{m,n} r)\, \mathrm{e}^{-\mathrm{j}(m\vartheta + k_z^{m,n} z)}, \qquad (2)$$

where r, θ and z are the radial, azimuthal and axial coordinates for the cylindrical geometry (the z-axis being along the pipe axis); and where m and n indicate the azimuthal and radial order of the mode, respectively. The amplitude of the mode is given by $A^{m,n}$. In equation (2) and the derivation from it which follows, the term $\mathrm{e}^{\mathrm{j}\omega t}$ has been suppressed. The Bessel function J_m is of the first kind, having integer order m. The radial and axial wavenumbers are $\kappa_{m,n}$ and $k_z^{m,n}$ respectively, related through

$$k_z^{m,n} = \sqrt{k^2 - (\kappa_{m,n})^2}, \qquad (3)$$

where the acoustic wavenumber k equals the ratio of the acoustic circular frequency ω to the sound speed c. The only modes which will propagate are those for which $k_z^{m,n}$ is real: If $\kappa_{m,n} > k$, that mode will be evanescent, giving a cut-off frequency for each mode below which an oscillating pressure field will not propagate. The total pressure field, if only forward-propagating modes exist, is given by an appropriate modal summation:

$$p_{tot}(r,\vartheta,z) = \sum_{m=-\infty}^{\infty} \sum_{n=0}^{\infty} A^{m,n} J_m(\kappa_{m,n} r)\, \mathrm{e}^{-\mathrm{j}(m\vartheta + k_z^{m,n} z)}. \qquad (4)$$

The radial particle velocity $u_r^{m,n}$ associated with each mode can be found by application of the conservation of linear momentum in the radial direction through

$$\frac{\partial u_r^{m,n}}{\partial t} = -\frac{1}{\rho}\frac{\partial p^{m,n}}{\partial r}, \qquad (5)$$

where ρ is the liquid density, to give

$$u_r^{m,n}(r,\vartheta,z) = -\frac{\kappa_{m,n} A^{m,n}}{\mathrm{j}\omega\rho}\frac{\partial J_m}{\partial r}\, \mathrm{e}^{-\mathrm{j}(m\vartheta + k_z^{m,n} z)}. \qquad (6)$$

If Z is the acoustic impedance at the pipe wall, then

$$Z = \left.\frac{p^{m,n}}{u_r^{m,n}}\right|_{r=a}. \qquad (7)$$

If the pipe wall is a pressure-release surface, then $p^{m,n}$ must be zero at $r = a$, giving from equation (5) the boundary condition that:

$$J_m(\kappa_{m,n} a) = 0. \qquad (8)$$

If the pipe wall were to be rigid, then $u_r^{m,n}$ must be zero at $r = a$, giving from equation (2) the boundary condition that:

$$J'_m(\kappa_{m,n} a) = 0. \qquad (9)$$

The pipe has an inner radius of 52 mm, and an outer one of 58 mm. If is assumed that the pipe is bounded by a pressure release surface at a radius of 58 mm, then given the range of acoustic frequencies of 3.5 to 5 kHz, it is possible to use equations (3), (8) and (9) to determine which modes will propagate. Assuming a sound speed of 1420 m/s in the water, then ka takes values of 0.90 and 1.28 at frequencies of 3.5 and 5 kHz respectively. Regarding propagation in the axial direction in a pipe having a pressure-release wall, the first zero in J_0 occurs at $kr = 2.405$ (and if the wall were rigid, the first zero in $\partial J_0/\partial r$ for finite kr occurs at $kr = 3.83$). Therefore, given that the pipe in question is approximately pressure-release at the wall, then the frequency range investigated is below cut-off, and all waves are evanescent in the axial direction.

Were measurements to be made at higher frequencies, other acoustic effects must be considered. As the frequency increases, the modes become more closely spaced in frequency. Since each mode has a certain bandwidth, then at some frequency (termed the Schroeder frequency) their overlap will be such that the sound field resembles diffuse conditions [51], so that excitation at a single frequency involves the response from many modes. At intermediate frequencies, the field is characterised by distinct modes[1] in the cross-section of the pipe, and these must be accounted for unless either (i) it can be assured that the amplitude of the pump sound field at the position of the bubble is known; or (ii) amplitude information is not required (i.e. only the presence, and not the absolute number, of bubbles is to be monitored), and it can be assured that the bubble will not occur at a minimum of the sound field. Both (i) and (ii) can be brought about if the combination frequency technique is used to sample the bubble population in the pipe, so that only the amplitude of the pump field at the high-frequency focus is important.

How well a given circumstance reflects the case of the infinitely-long pipe discussed above is case-specific. Reflections may occur at bends and junctions, giving rise to waves which propagate in the $-z$ direction. The experiment described in this paper used, not an infinitely-long pipe, but a cylindrical volume of length 0.5 m. The existence of modes in the axial direction in such an experiment requires consideration. The water-filled section of the pipe was length $L = 0.5$ m long. The upper-surface was an air-water interface, and axial waves would insect this normal to the direction of propagation, with a nearly pressure-release boundary condition. The lower boundary will be similar to that of the pipe walls. Making the approximation of pressure release ends, the axial mode of order q will therefore have a resonance frequency of $qc/2L$, corresponding to 1420, 2840 Hz. . . , i.e. a mode exists every 1420 Hz. Clearly therefore in our experiment the amplitude of the pump signal would be affected by the existence of axial modes, and for this reason the calibration procedure described in section 2 was performed. It was simple, using this, to ensure that the pump signal amplitude at

[1] It should be noted that bubble detection systems have been produced which exploit acoustic modes [52], and such a system may be possible in a pipe at certain frequencies.

ACUSTICA · acta acustica
Vol. 84 (1998)

any bubble that was detected by the combination-frequency technique was known and constant, and could be experimentally maintained. The importance of this will now be discussed.

In our experiment, the bubbles were confined to the region of the high frequency transducer focus (as confirmed by the use of the Hitachi scanner). If the bubble detection is confined to the axis of the ring transducer, where the high frequency beams intersect (termed the 'focus'), then the calibration of the pump signal relates to its amplitude in that small region of the high frequency focus. As regards the calibration therefore, spatial variations in the pump field outside the focus will not cause a significant problem. However there other considerations: if one uses combination-frequency techniques for bubble detection, then only those bubbles which pass through the focus will be detected. Three options for deployment in a pipe are available. First, the beam intersection could be made as large as the pipe cross-section, through appropriate transducer design or (since near-field and wall reflections would complicate the field) the inclusion of a stand-off distance. This might be done, for example by incorporating the transducers into an annulus such that the beam propagates through a sufficient depth of material before entering the pipe to encompass the near field; and at the extreme wall of the pipe, the beam meets an anechoic termination. This however has implications for the uniformity of the amplitude of the pump signal throughout the focus. Second, the focus can cover only a region of the pipe as in the tests described, such that regions of the flow will be unmonitored: consideration of the output of the bubble detector must recognise that this sampling process has occurred. Third, enough high frequency beams can be paired (although a single emitter beam can be paired with several detectors) to produce a number of foci sufficient to cover that proportion of the pipe cross section which is deemed to be appropriate for the degree of sampling. Which option is chosen depends on cost, sampling requirements and, most interesting to this study, the information that is required of the bubble population. If the object is to detect the presence of bubbles, and obtain an indication of the bubble sizes present, but not to count the bubbles beyond a simple 'none-some-many' categorisation, then the amplitude of the pump signal in the focus is not critical. Many common industrial situations (e.g. material processing), where the usual running situation should be bubble-free and the detection of a bubble indicates malfunction, require only this level of sophistication. If, however, the object is also to count the bubbles, then the most reliable technique for doing this is the use of the $\omega_i \pm \omega_p$ signal [41], the amplitude of which can be related to the number of bubbles of a given size. This is particularly so for dense bubble populations. In the ocean, bubble densities of 10^6 per m^3 per μm radius increment have been measured [41], although if the occurrence of such high number densities of bubbles represented catastrophic failure to a given industry, then simple detection (as opposed to counting) would suffice. Similarly, the fact that certain counting errors increase with increasing population densities (e.g. because of multiple-scattering) would be of secondary importance in the detection of catastrophic failure. If however a reliable bubble count is required, given that the amplitude of the pump signal will vary across the pipe cross-section, it is important to ensure its amplitude is roughly constant (the less so, the greater the error bars in the count) and known across the focus/foci. This is clearly possible for the second and third options outlined above, but not for the first.

4.3. Estimating the bubble size from its resonance frequency

At low frequencies the acoustic radiation impedance of a pulsating sphere of radius R_0 in free space, Z_s, is given by [53, 1]:

$$Z_s \approx \frac{\rho\omega^2}{4\pi c} + \frac{\mathrm{j}\rho\omega}{4\pi R_0} \quad (kR_0 \ll 1), \tag{10}$$

where ρ and c are, respectively, the density and sound speed in the liquid; and the acoustic field has wavenumber k and circular frequency ω. The low frequency condition means that $kR_0 \ll 1$. The imaginary term dominates, such that the radiation reactance (i) is much greater than the radiation resistance, and (ii) is mass-like, contributing an inertia associated with the liquid motion around the pulsating sphere of

$$m_r = \left(4\pi R_0^2\right)^2 \Im m\{Z_d\}/\omega = 4\pi R_0^3 \rho. \tag{11}$$

The natural frequency of the bubble can be estimated, as stated in the introduction, through comparison between the potential energy invested in the gas and the kinetic energy associated with the motion of the liquid; or, equivalently, from the root of the ratio of the stiffness of the gas s, to the radiation mass. Since

$$s = 12\pi K P_0 R_0 \tag{12}$$

(where K is the polytropic index of the gas, and P_0 is the static pressure at the bubble), then comparison of equations (11) and (12) shows that the natural frequency of the bubble is

$$\nu_0 = \frac{1}{2\pi}\sqrt{\frac{s}{m_r}} = \frac{1}{2\pi R_0}\sqrt{\frac{3KP_0}{\rho}}. \tag{13}$$

This derivation neglects the effects of surface tension and viscosity, but is relevant for air bubbles having $R_0 \gtrsim 10\,\mu$m in an infinite body of water. If $P_0 \equiv 1$ atmosphere, equation (13) reduces to equation (1) as discussed in the introduction.

More generally, let Z_b be the acoustic impedance of the bubble, that is, the ratio of the pressure change ΔP to the inwards volume velocity at the bubble wall, $-U$. If Z_a is the external acoustic impedance due to fluid loading on the bubble, then resonance occurs when

$$Z_a + Z_b = 0. \tag{14}$$

This can be used to determine the relationship between the bubble pulsation resonance and the bubble radius. For example, since the bulk modulus of the gas within the bubble

is $B = -V\Delta P/\Delta V$, then assuming single-frequency simple harmonic motion at circular frequency ω, the acoustic impedance of the bubble is

$$Z_b \approx \frac{\Delta P}{-U} = \frac{\Delta P}{-\mathrm{j}\omega\Delta V} = \frac{B}{\mathrm{j}\omega V}. \tag{15}$$

The resonance relation can be found for the given assumed conditions. For example, consider if Z_s from equation (10) is used to represent Z_a in equation (14), and its resistive component is assumed to be negligible in comparison with the reactive term. If in addition the gas within the spherical bubble is assumed to behave polytropically, such that $B = KP_0$, then substitution for Z_b, from (15) into (14), gives the prior result (equation (13)). If damping is included in the expressions for Z_a and Z_b, then the bulk modulus is complex, and the formulation gives the decay constant.

Equation (10) represents the pulsation of a bubble in free space. If however the bubble is in a pipe, then the natural frequency of the bubble will differ from that given by (13). This is because the body of liquid surrounding the bubble is neither infinite nor moves with spherical symmetry, and because the pipe walls impose boundary conditions and generate reflections. Consider a bubble of radius R_0 in an infinitely-long pipe of radius a. It is pulsating at its natural frequency, and so generates a pressure field of wavenumber k. A cylindrical co-ordinate system (r, ϑ, z) has the z-axis co-linear with the pipe axis. The pressure field radiated by the bubble p consists of a direct field p_d and a reverberant field p_v, such that

$$p = p_d + p_v. \tag{16}$$

At frequencies such that $kR_0 \ll 1$ (valid for this experiment), the reverberant field p_v will be virtually constant over the bubble surface, and virtually the same as that produced at the bubble centre location by a point source having the same volume velocity as the bubble.

It is necessary to find the total acoustic impedance Z presented to the bubble by its environment, given by

$$Z = \frac{p}{U} = \frac{p_d}{U} + \frac{p_v}{U}, \tag{17}$$

where U is the volume velocity. The contribution to this from the reverberant field is

$$Z_v = \frac{p_v}{U} \tag{18}$$

and may significantly influence the total, even if the bubble is not close to a wall. However, from the above comments, Z_v is not expected to be a function of the bubble radius, R_0, in the limits of $kR_0 \ll 1$ and $R_0 \ll a$.

The contribution from the direct field is

$$Z_d = \frac{p_d}{U} \approx \frac{\rho\omega^2}{4\pi c} + \frac{\mathrm{j}\rho\omega}{4\pi R_0} \quad (kR_0 \ll 1), \tag{19}$$

i.e. equal to Z_s (equation 10). Consider the pipe to have pressure-release walls. Its Green function can be calculated following Morse and Ingard [54]. The pipe acoustic Green function, $G(\boldsymbol{x}|\boldsymbol{x}')$, is defined as the solution of

$$(\nabla^2 + k^2)G(\boldsymbol{x}|\boldsymbol{x}') = -\delta(\boldsymbol{x} - \boldsymbol{x}'), \tag{20}$$

which obeys an appropriate impedance boundary condition at $r = a$ (the inner pipe wall) and yields outgoing waves at $z = \pm\infty$ (corresponding to an unbounded pipe). The Green function can be expressed in terms of the acoustic-mode eigenfunctions $\psi_n(\boldsymbol{y})$ which are orthogonal functions of the transverse position $\boldsymbol{y}$:

$$\int \psi_n(\boldsymbol{y})\psi_{n'}(\boldsymbol{y})\,\mathrm{d}S(\boldsymbol{y}) = \begin{cases} 0, & n' \neq n, \\ \Lambda_n S, & n' = n, \end{cases} \tag{21}$$

where S is the cross-sectional area of the pipe and Λ_n is the normalisation constant for a particular mode. The eigenfunctions satisfy the two-dimensional Helmholtz equation:

$$(\nabla_z^2 + \kappa_n^2)\psi_n = 0 \tag{22}$$

together with the pipe wall boundary condition (which is in this case taken to be pressure-release, making the κ_n real). Then, as discussed above, below the cut-off frequency of the first mode, $k < \kappa_1$ and all modes decay axially with a factor:

$$\mathrm{e}^{-\gamma_n|z-z'|}, \qquad \gamma_n = \sqrt{\kappa_n^2 - k^2}. \tag{23}$$

With the above notation, the exact Green's function is given by

$$G(\boldsymbol{x}|\boldsymbol{x}') = \frac{1}{2S}\sum_n \frac{1}{\Lambda_n\gamma_n}\psi_n(\boldsymbol{y})\psi_n(\boldsymbol{y}')\,\mathrm{e}^{-\gamma_n|z-z'|}, \tag{24}$$

where the sum extends over all modes. Equation (9) holds for $ka < 2.405$, as explained above.

It is now possible to obtain a low-frequency approximation to the Green's function, valid when ka is of order 1 or less, in the form of a series which can be truncated after a few terms without significant error. It relies on the fact that the reverberant-field pressure p_v does not vary significantly over distances of order R_0 when $kR_0 \ll 1$; therefore, if $\boldsymbol{x}_0$ is the position of the bubble centre, at points on the bubble surface given by

$$\boldsymbol{x} = \boldsymbol{x}_0 + \boldsymbol{R}_0 \tag{25}$$

the reverberant-field contribution G_v to the Green's function G can be estimated as

$$G_v(\boldsymbol{x}|\boldsymbol{x}_0) \approx G_v(\boldsymbol{x}_0|\boldsymbol{x}_0) \qquad (kR_0 \ll 1) \tag{26}$$

for a point source at the bubble centre. Taking the limit $ka \to 0$ in the exact Green's function as given by equation (24) yields the following exact equivalence as the distance $|\boldsymbol{x} - \boldsymbol{x}'|$ is made vanishingly small:

$$\frac{1}{4\pi R_0} = \frac{1}{2S}\sum_n \frac{1}{\Lambda_n\gamma_n}\psi_n(\boldsymbol{y})\psi_n(\boldsymbol{y}')\,\mathrm{e}^{-\kappa_n|z-z'|}, \tag{27}$$

where $\boldsymbol{R}_0 = |\boldsymbol{x} - \boldsymbol{x}'|$. Combining equations (24) and (27) gives

$$G(\boldsymbol{x}|\boldsymbol{x}') = \frac{1}{4\pi R_0} + \frac{1}{2S}\sum_n \frac{1}{\Lambda_n}\psi_n(\boldsymbol{y})\psi_n(\boldsymbol{y}') \cdot \left[\frac{1}{\gamma_n}\mathrm{e}^{-\gamma_n|z-z'|} - \frac{1}{\kappa_n}\mathrm{e}^{-\kappa_n|z-z'|}\right]. \tag{28}$$

ACUSTICA · acta acustica
Vol. 84 (1998)

Although this still represents an infinite sum, its evaluation is simplified in that (i) the terms decay rapidly with increasing n because of the factor in square brackets; and (ii) the singularity at $R_0 = 0$ has been removed from the summation, being represented now by the $(4\pi R_0)^{-1}$ term.

Invoking the approximation (26) for the reverberant field gives, for points $\boldsymbol{x}$ on the bubble surface,

$$G(\boldsymbol{x}|\boldsymbol{x}_0) \approx \frac{1}{4\pi R_0} + \frac{1}{2S}\sum_n \frac{1}{\Lambda_n}\psi_n^2(\boldsymbol{y})\left[\frac{1}{\gamma_n} - \frac{1}{\kappa_n}\right]. \quad (29)$$

Equation (29) is valid below the first transverse-mode cut-off frequency in a cylinder with pressure-release walls ($ka < 2.405$) and for $k|\boldsymbol{x} - \boldsymbol{x}_0| \ll 1$. Using it, it is now possible to obtain the correction to the fluid loading impedance at the surface of a small bubble which allows for the fact that the bubble is confined in a pipe under these circumstances, as opposed to free-field. The first term of equation (29) gives the standard free-field reactive loading impedance for $kR_0 \ll 1$, i.e.

$$Z_d \approx \frac{\mathrm{j}\rho\omega}{4\pi R_0} \qquad (kR_0 \ll 1), \quad (30)$$

(compare with equation (19) in the stated limits). The infinite modal series in equation (29) gives the reverberant-field correction:

$$Z_v \approx \frac{\mathrm{j}\rho\omega}{2S}\sum_n \frac{1}{\Lambda_n}\psi_n^2(\boldsymbol{y}_0)\left[\frac{1}{\gamma_n} - \frac{1}{\kappa_n}\right], \quad (31)$$

where $\boldsymbol{y}_0$ is the transverse location of the bubble centre in the pipe. Equation (31) is valid for frequencies below the first mode cut-off. In the undamped condition, when cut-off is reached ($\gamma_1 = 0$ when $k = \kappa_1$), Z_v becomes infinite, corresponding to modal resonance. To obtain a better estimate close to such resonances, wall damping (including radiation damping) should be included.

The ratio of the reverberant field impedance to that of the direct field is given by:

$$\frac{Z_v}{Z_d} \approx \frac{2\pi R_0}{S}\sum_n \frac{1}{\Lambda_n}\psi_n^2(\boldsymbol{y}_0)\left[\frac{1}{\gamma_n} - \frac{1}{\kappa_n}\right] \equiv \frac{2R_0}{a}\sum_n \frac{1}{\Lambda_n}\psi_n^2(\boldsymbol{y}_0)\left[\frac{1}{\gamma_n a} - \frac{1}{\kappa_n a}\right] \quad (32)$$

(where $\kappa_n a$ are the zeros of the Bessel functions) and characterises the effect of reverberation. Figure 7 shows a plot of $(Z_v/Z_d)/(R_0/a)$ within the above conditions, as a function of the sound frequency (which need not be in resonance with the bubble), for an infinitely long pipe of internal radius 58 mm, bounded by a pressure-release surface. It is clear that the effect of reverberation is small below the frequency of the first mode (where $m = 0$ and $n = 1$). This mode has a calculated frequency of 9.77 kHz for pressure-release, undamped walls; and, for the real pipe, a measured frequency of 10±0.25 kHz. However the effect of reverberation becomes large as the frequency of the first mode is approached. The addition of damping to the wall of the pipe would ensure

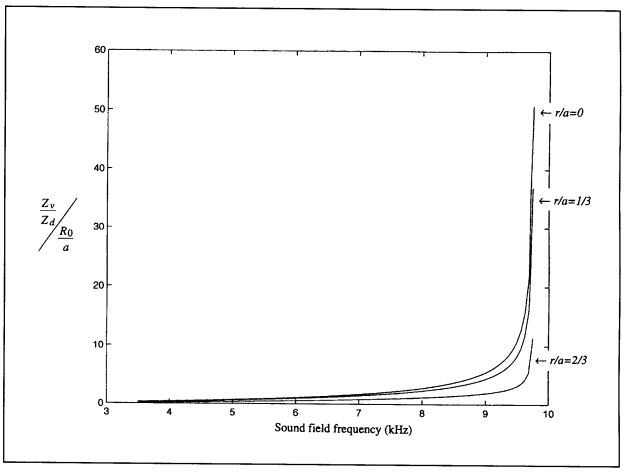

Figure 7. A plot of $(Z_v/Z_d)/(R_0/a)$ within the stated conditions, as a function of the sound frequency (which need not be resonant with the bubble), for an infinitely long pipe of radius 58 mm, bounded by a pressure-release surface. The curves relate to the bubble position being on-axis ($r/a = 0$) and off-axis ($r/a = 1/3, 2/3$).

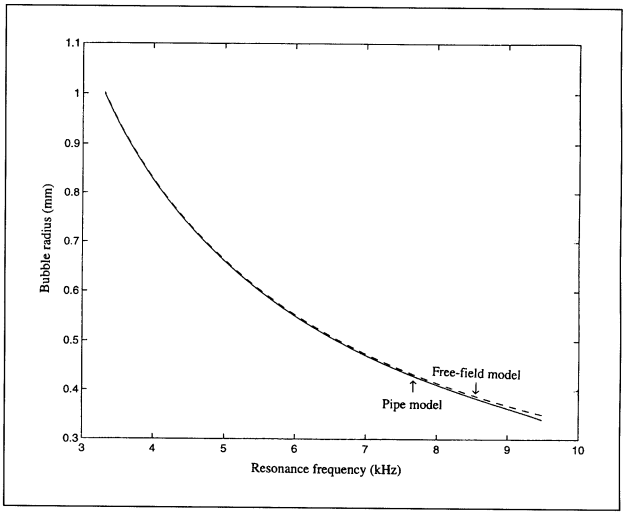

Figure 8. The figure shows the relation between resonance frequency and bubble size for: free-field conditions (from equation 13) shown by the dashed line; and for confinement on-axis within an infinitely long pipe (solid line) having a 58 mm radius and pressure-release walls (from equation 33). If the bubble were off-axis, the effect would be intermediate between these two extremes.

that Z_v/Z_d remains finite at the mode cutoff frequency. The plot is produced for both on-axis ($r/a = 0$) and two off-axis ($r/a = 1/3, 2/3$) bubble positions.

The resonance frequency of the bubble can therefore be calculated as

$$\nu_r \approx \frac{1}{2\pi}\sqrt{\frac{s\omega}{(4\pi R_0^2)^2 \Im m\{Z_d + Z_v\}}}. \quad (33)$$

The formulation requires iterative solution. Figure 8 shows the relation between resonance frequency and bubble size for free-field conditions (equation 13) and for confinement on-axis within the 58 mm radius, infinitely long pipe with pressure-release walls (equation 33). If the bubble were

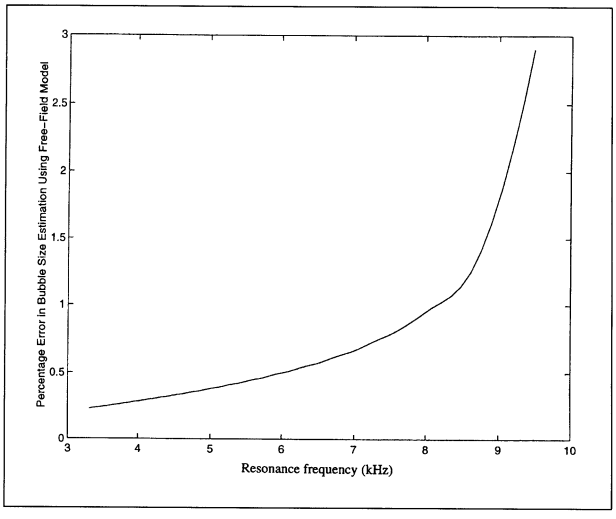

Figure 9. The figure shows the percentage error in the estimate of the bubble radius which would arise if formulations relevant to free-field conditions were to be used to convert a measured bubble resonance into a bubble radius, instead of applying equation (13). (Slight deviations from a smooth curve arise because of the iterative nature of the solution).

off-axis, the effect would be intermediate between these two extremes. As expected, greater deviation between the two curves is seen as the frequency of the first mode is approached. In this experiment a bubble resonance of 3950±50 Hz is detected. If this were in free-field, it would correspond to a bubble of radius 844±11 μm, whilst if the bubble were on-axis in the pipe, such a resonance frequency would suggest a bubble radius of 840±11 μm. Figure 9 shows the percentage error in the estimate of the bubble radius which would arise if formulations relevant to free-field conditions were to be used to convert a measured bubble resonance into a bubble radius, instead of applying equation (13). As can be seen, the error increases at frequencies approaching that of the first mode, but is less than 0.5% for the bubbles investigated in this test. If the absolute number of bubbles is to be quantified, then the effect on the damping of the sound which propagates above the frequency of the first mode must also be determined.

5. Conclusion

A liquid-filled pipe has been instrumented to investigate the air bubbles contained within it. It was envisaged that the simultaneous use of several acoustic signals would allow a degree of compensation for the limitations of the different individual techniques. The bubble location could be identified using a diagnostic ultrasonic imaging system, but this signal gave poor indication of the bubble size. To measure the latter, six acoustic signals (the generation of which are all influenced by the existence of the bubble resonance) were simultaneously examined. These six signals included components in both the direct scattered sound field, and in the field scattered from the bubble when insonified using a combination frequency technique. However for both tethered and rising bubbles, only three of these six signals provided useful data on the bubble size. These signals correspond, specifically: to direct acoustic scatter at the pump frequency by the bubble; and to combination-frequency signals due to the volumetric bubble pulsation, and due to surface waves at half the driving frequency. Discussion is given of the potential ambiguities and disadvantages of each signal, as well as of how the effects of pipe modes and the proximity to the pipe surfaces may affect the quality of the returned bubble information. A formulation has been provided which allows the calculation of the bubble resonance when the reverberant field in the pipe is taken into consideration. This has general implications for acoustic bubble sizing in reverberant conditions.

Acknowledgement

Dr. Leighton is grateful to the Natural Environment Research Council (grant ref: GR3/09992) for providing funding for Dr. Phelps, and to the Engineering and Physical Sciences Research Council (grant ref: GR/H 79815) for providing funding for Dr. Ramble. The authors wish to thank Dr. D. Hewlett for useful discussion and Mr. J. Clarke for assistance with the figures.

References

[1] T. G. Leighton: The acoustic bubble. Academic Press, London, 1994, 146-147.
[2] T. G. Leighton: Acoustic bubble detection I. - the detection of stable gas bodies. J. Soc. Env. Eng. **7** (1994) 9–16.
[3] R. M. Detsch, R. N. Sharma: The critical angle for gas bubble entrainment by plunging liquid jets. The Chemical Engineering Journal (1990) 157–166.
[4] E. G. Tickner: Precision microbubbles for right side intercardiac pressure and flow measurements. – In: Contrast Echocardiography. R. S. Meltzer, J. Roeland (eds.). Nijhoff, London, 1982.
[5] S. A. Thorpe: Measurements with an automatically recording inverted echo sounder; ARIES and the bubble clouds. J. Physical Oceanography **16** (1986) 1462–1478.
[6] D. K. Woolf: Bubbles and the air-sea transfer velocity of gases. Atmos-Ocean **31** (1993) 451–474.
[7] E. A. Neppiras: Acoustic cavitation. Phys. Rep. **61** (1980) 159–251.
[8] R. E. Apfel, C. K. Holland: Gauging the likelihood of cavitation from short-pulse, low-duty cycle diagnostic ultrasound. Ultrasound in Medicine and Biology **17** (1991) 179–185.
[9] T. G. Leighton: Acoustic bubble detection II. - the detection of transient cavitation. J. Soc. Env. Eng. **8** (1995) 16–25.
[10] T. G. Leighton: Bubble population phenomena in acoustic cavitation. Ultrasonics Sonochemistry **2** (1995) 123–136.
[11] J. Wolf: Investigation of bubbly flow by ultrasonic tomography. Part. Sys. Charact. **5** (1988) 170–173.
[12] S. L. Morriss, A. D. Hill: Ultrasonic imaging and velocimetry in two-phase pipe flow. Trans. ASME **115** (1993) 108–116.
[13] R. Y. Nishi: Ultrasonic detection of bubbles with Doppler flow transducers. Ultrasonics **10** (1972) 173–179.
[14] A. Lubbert, T. Korte, K. Schuegerl: Ultrasonics Doppler measurements of bubble velocities in bubble columns. I.U.T.A.M. Symposium on Measuring Technology in Gas-Liquid Two-Phase flows, Nancy, France, 1983. 479–494.
[15] A. Lubbert, T. Korte, B. Larson: Simple measuring techniques for the determination of bubble and bulk phase velocities in bioreactors. Applied Biochemistry and Biotechnology **14** (1986) 207–219.

[16] E. O. Belcher: Quantification of bubble formation in animals and man during decompression. I.E.E.E. Transactions on Biomedical Engineering **27** (1980) 330–338.
[17] R. S. MacKay, J. R. Rubisson: Decompression studies using ultrasonic imaging of bubbles. I.E.E.E. Transactions on Biomedical Engineering **25** (1978) 537–544.
[18] D. J. Watmough, H. M. Davies, K. M. Quan, R. Wytch, A. R. Williams: Imaging microbubbles and tissues using a linear focused scanner operating at 20 mhz: possible implications for the detection of cavitation thresholds. Ultrasonics **29** (1991) 312–318.
[19] L. Matikainen, G. A. Irons, E. M. Morala, J.-S. Chang: Ultrasonic system for the detection of transient liquid/gas interfaces using the pulse-echo technique. Rev. Sci. Instum. **57** (1986) 1661–1666.
[20] A. A. Stravs, J. Wahl, U. V. Stockar, P. J. Reilly: Development of an ultrasonic pulse reflection method for measuring relative size distributions of air bubbles in aqueous solutions. Chemical Engineering Science **42** (1987) 1677–1688.
[21] J. S. ChAng, E. C. Morala: Determination of two-phase interfacial areas by an ultrasonic technique. Nuclear Engineering and Design **122** (1990) 143–156.
[22] W. F. Kolbe, B. T. Turko, B. Leskovar: Fast ultrasonic imaging in a liquid filled pipe. I.E.E.E. Transactions on Nuclear Science **33** (1986) 715–722.
[23] B. T. Turko, W. F. Kolbe, B. Leskovar: Ultrasonic system for imaging of vapor bubbles in a liquid filled pipe. I.E.E.E. Transactions on Nuclear Science **33** (1986) 1115–1122.
[24] S. J. Norton, M. Linzer: Ultrasonic reflectivity tomography: reconstruction with circular transducer arrays. Ultrasonic Imaging **1** (1979) 154–184.
[25] S. J. Norton: Reconstruction of a reflectivity field from line integrals over circular paths. J. Acoust. Soc. Am. **67** (1980) 853–863.
[26] S. J. Norton: Reconstruction of a two-dimensional reflecting medium over a circular domain: Exact solution. J. Acoust. Soc. Am. **67** (1980) 1266–1273.
[27] H. Gai: Ultrasonic techniques for flow imaging. Dissertation. U.M.I.S.T., England, 1990.
[28] F. Wiegand, B. S. Hoyle: Simulations for parallel processing of ultrasound reflection-mode tomography with applications to two-phase flow measurement. I.E.E.E. Transactions on Ultrasonics, Ferroelectrics and Frequency Control **36** (1989) 652–660.
[29] F. Wiegand, B. S. Hoyle: Development and implementation of real-time ultrasound process tomography process tomography using a transputer network. Paralleled Computing **17** (1991) 791–807.
[30] J. M. Blackledge: B-scan imaging of two phase flows. IEE Colloquium on Ultrasound in the process industry, September 23rd, 1993. 5/1–5/17.
[31] S. A. Thorpe, A. J. Hall: The characteristics of breaking waves, bubble clouds and near-surface currents observed using side-scan sonar. Continental shelf Research **1** (1983) 353–384.
[32] J. S. Chang, Y. Ichikawa, G. A. Irons, E. C. Morala, P. T. Wan: Void fraction measurement by an ultrasonic transmission technique in bubbly gas-liquid two-phase flow. I.U.T.A.M. Symposium on Measuring Technology in Gas-Liquid Two-Phase flows, Nancy, France, 1983. 319–335.
[33] A. A. Stravs, U. V. Stockar: Measurement of interfacial areas in gas-liquid dispersions by ultrasonic pulse transmission. Chemical Engineering Science **40** (1985) 1169–1175.
[34] M. Minnaert: On musical air-bubbles and sounds of running water. Phil. Mag. **16** (1933) 235–248.
[35] M. Strasberg: The pulsation frequency of nonspherical gas bubbles in liquids. J. Acoust. Soc. Am. **25** (1953) 536–537.
[36] M. S. Longuet-Higgins: The sound field due to an oscillating bubble near an indented free surface. J. F. Mech. **221** (1990) 675–683.
[37] H. N. Oguz, A. Prosperetti: Bubble oscillations in the vicinity of a nearby plane free surface. J. Acoust. Soc. Am. **87** (1990) 2085–2092.
[38] T. G. Leighton, P. R. White, M. A. Marsden: Applications of one-dimensional bubbles to lithotripsy, and to diver response to low frequency sound. Acta Acustica **3** (1995) 517–529.
[39] H. Medwin: Counting bubbles acoustically: a review. Ultrasonics **15** (1977) 7–14.
[40] T. G. Leighton, A. D. Phelps, D. G. Ramble: Acoustic bubble sizing: from laboratory to the surf zone trials. Acoustics Bulletin **21** (1996) 5–12.
[41] A. D. Phelps, D. G. Ramble, T. G. Leighton: The use of a combination frequency technique to measure the surf zone bubble population. J. Acoust. Soc. Am. **101** (1997) 1981–1989.
[42] A. D. Phelps, T. G. Leighton: High resolution bubble sizing through detection of the subharmonic response with a two frequency excitation technique. J. Acoust. Soc. Am. **99** (1996) 1985–1992.
[43] T. G. Leighton, D. G. Ramble, A. D. Phelps: The detection of tethered and rising bubbles using multiple acoustic techniques. J. Acoust. Soc. Am. **101** (1997) 2626–2635.
[44] R. Clift, J. R. Grace, M. E. Weber: Bubbles, drops and particles. Academic Press, New York, 1978.
[45] P. N. T. Wells: Biomedical ultrasonics. Academic Press, London, 1977, 207-222.
[46] H. Kuttruff: Ultrasonics, fundamentals and applications. Elsevier Applied Science, London and New York, 1991, 306-8.
[47] A. D. Phelps, T. G. Leighton: The subharmonic oscillations and combination-frequency subharmonic emissions from a resonant bubble: their properties and generation mechanisms. Acta Acustica **83** (1997) 59–66.
[48] A. D. Phelps: Characterisation of the subharmonic response of a resonant bubble using a two frequency technique. Dissertation. University of Southampton, UK, 1995.
[49] T. G. Leighton, A. D. Phelps, D. G. Ramble, D. A. Sharpe: Comparison of the abilities of eight acoustic techniques to detect and size a single bubble. Ultrasonics **34** (1996) 661–667.
[50] H. Medwin: In situ acoustic measurements of microbubbles at sea. J. Geophys. Res. **82** (1977) 971–976.
[51] A. D. Pierce: Acoustics - An introduction to its physical principles and applications. McGraw-Hill, Inc., New York, 1981, 294.
[52] H. Medwin, N. D. Breitz: Ambient and transient bubble spectral densities in quiescent seas and under spilling breakers. J. Geophys. Res. **94** (1989) 12751–12759.
[53] L. E. Kinsler, A. R. Frey, A. B. Coppens, J. V. Sanders: Fundamentals of acoustics. John Wiley and Sons, Inc., 1982, 191-193, 228-229.
[54] P. M. Morse, K. U. Ingard: Theoretical acoustics. Princeton University Press, Princeton, New Jersey, 1986, 500-503.
[55] D. Koller, Y. Li, P. M. Shankar, V. L. Newhouse: High-speed bubble sizing using the double frequency technique for oceanographic applications. IEEE J. Oceanic Engineering **17** (1992) 288–291.
[56] D. L. Miller: Ultrasonic detection of resonant cavitation bubbles in a flow tube by their second harmonic emissions. Ultrasonics **19** (1981) 217–224.
[57] D. L. Miller, A. R. Williams, D. R. Gross: Characterisation of cavitation in a flow-through exposure chamber by means of a resonant bubble detector. Ultrasonics **22** (1984) 224–230.
[58] A. D. Phelps, T. G. Leighton: Investigations into the use of two frequency excitation to accurately determine bubble sizes. – In: Bubble Dynamics and Interface Phenomena. Proceedings of an IUTAM symposium held in Birmingham, UK, 6-9 September 1993. J. R. Blake et al. (eds.). Kluwer Academic Press, Netherlands, 1994, 475–483.